Ambient Light Resistant Shortwave Infrared Fluorescence Imaging for Preclinical Tumor Delineation via the pH Low-Insertion Peptide Conjugated to Indocyanine Green

Benedict Edward Mc Larney[1], Mijin Kim*[1], Sheryl Roberts*[2], Magdalena Skubal*[1], Hsiao-Ting Hsu[1], Anuja Ogirala[1], Edwin C. Pratt[1,2], Naga Vara Kishore Pillarsetty[2,4], Daniel A. Heller[1,3], Jason S. Lewis[1–4], and Jan Grimm[1–5]

[1]*Molecular Pharmacology Program, Memorial Sloan Kettering Cancer Center, New York, New York;* [2]*Department of Radiology, Memorial Sloan Kettering Cancer Center, New York, New York;* [3]*Department of Pharmacology, Weill Cornell Medicine, New York, New York;* [4]*Department of Radiology, Weill Cornell Medicine, New York, New York; and* [5]*Molecular Imaging Therapy Service, Memorial Sloan Kettering Cancer Center, New York, New York*

Shortwave infrared (900–1,700 nm) fluorescence imaging (SWIRFI) has shown significant advantages over visible (400–650 nm) and near-infrared (700–900 nm) fluorescence imaging (reduced autofluorescence, improved contrast, tissue resolution, and depth sensitivity). However, there is a major lag in the clinical translation of preclinical SWIRFI systems and targeted SWIRFI probes. **Methods:** We preclinically show that the pH low-insertion peptide conjugated to indocyanine green (pHLIP ICG), currently in clinical trials, is an excellent candidate for cancer-targeted SWIRFI. **Results:** pHLIP ICG SWIRFI achieved picomolar sensitivity (0.4 nM) with binary and unambiguous tumor screening and resection up to 96 h after injection in an orthotopic breast cancer mouse model. SWIRFI tumor screening and resection had ambient light resistance (possible without gating or filtering) with outstanding signal-to-noise ratio (SNR) and contrast-to-noise ratio (CNR) values at exposures from 10 to 0.1 ms. These SNR and CNR values were also found for the extended emission of pHLIP ICG in vivo (>1,100 nm, 300 ms). **Conclusion:** SWIRFI sensitivity and ambient light resistance enabled continued tracer clearance tracking with unparalleled SNR and CNR values at video rates for tumor delineation (achieving a tumor-to-muscle ratio above 20). In total, we provide a direct precedent for the democratic translation of an ambient light resistant SWIRFI and pHLIP ICG ecosystem, which can instantly improve tumor resection.

Key Words: SWIR; fluorescence; surgery; preclinical; tumor

J Nucl Med 2023; 64:1647–1653
DOI: 10.2967/jnumed.123.265686

Shortwave infrared (SWIR, 900–1,700 nm, or the second near-infrared [NIR] window) fluorescence imaging (SWIRFI) is providing novel insights for preclinical and clinical biophotonic imaging (*1–5*). In the SWIR spectrum, tissue scattering, absorption, and autofluorescence are negligible, permitting higher contrast, deeper penetration, and improved resolution (*6–10*). By combining the spectral response of human eyes (380–720 nm) with SWIR detector insensitivity below 920 nm, SWIRFI can be performed without ambient light removal and with no effect on human vision (*11*). SWIRFI is undergoing rapid preclinical deployment but is hampered by system and dye unavailability for routine applications that are investigating complex and diverse biologic systems, a situation that is exacerbated in clinical settings. SWIRFI has characterized the extended emission of indocyanine green (ICG, >900 nm, which is invisible to silicon sensors), with improvements in resolution and contrast over silicon-based NIR fluorescence imaging (NIRFI) (*5*,*8*,*10*,*12–14*). Improved spatial resolution can be achieved with SWIRFI by using long-pass filters at 1,100 and 1,300 nm, and simply using the entire SWIRFI spectral response enables improved image quality over NIRFI (*15*). In addition, dedicated SWIR (>1,000 nm) fluorophores have been developed (*16*,*17*). Targeted clinical cancer resection could greatly benefit from SWIRFI, but novel SWIRFI cancer-targeting agents require further assessment before clinical deployment (*11*,*16*,*18*). Accordingly, clinical SWIRFI has focused on the nontargeted enhanced permeability and retention effect (second window) of ICG-based imaging. Here, SWIRFI has shown both image and patient outcome improvements over NIRFI for liver tumor surgery, glioma resection, cystic renal mass removal, and brain metastasis (*19–22*). However, there is an unmet need for a workhorse cancer-targeting agent for SWIRFI like that of ^{18}F-FDG for PET (*23*).

The pH low-insertion peptide (pHLIP) conjugated to ICG (pHLIP ICG), not yet validated for SWIRFI, is a tumor-targeting agent under clinical investigation for breast cancer resection (NCT05130801) (*24–27*). In acidic tumor microenvironments, pHLIP ICG inserts into cellular membranes, displays high selectivity and contrast over healthy tissues, and preclinically delineates various cancers (*24*). pHLIP is also amenable to other dyes or radiolabeling (*28*,*29*). Here, we combined commercial SWIRFI's video rate picomolar sensitivity to ICG with the tumor selectivity of pHLIP ICG. We achieved video rates with a high signal-to-noise ratio (SNR), a high contrast-to-noise ratio (CNR), and preclinical tumor screening and resection in an orthotopic murine breast model. SWIRFI displayed improved sensitivity over the current preclinical gold-standard NIRFI (IVIS; PerkinElmer) for pHLIP ICG, extending the video-guided surgical resection window from 24 up to 96 h (*24*,*30–32*). Surgical window extension enabled an increased tumor CNR, peaking 72–96 h after injection, with tumor screening and resection possible at exposures of 10–0.1 ms. This could be performed under cost-effective and facile ambient lighting conditions (no gating), enhancing clinical practicality, translation, and dissemination (*33*). The extended

Received Mar. 6, 2023; revision accepted Jun. 12, 2023.
For correspondence or reprints, contact Benedict Edward Mc Larney (mclarneb@mskcc.org) or Jan Grimm (grimmj@mskcc.org).
*Contributed equally to this work.
Published online Aug. 24, 2023.

emission of pHLIP ICG beyond 1,100 nm in vivo is also demonstrated. The CNR achieved by SWIRFI (mean tumor-to-muscle ratio of 22.6) provided binary and unambiguous tumor or no-tumor delineation, with implications for preclinical assessment of other cancer-targeting dyes. This work establishes the basis for SWIRFI's clinical translation via pHLIP ICG for targeted cancer resection, aiding the translation of other SWIRFI cancer-targeting agents.

MATERIALS AND METHODS

Ambient Light Resistant SWIRFI

A commercial preclinical SWIR hyperspectral system (IR-VIVO and PHySpec; Photon Etc.) permitted in vivo SWIRFI. Laser excitation (808 nm) was distributed over the mouse (90–450 mW/cm^2, measured using a laser power meter, PM100D; Thorlabs). Sensor settings were −70.0°C, high gain, 0 gain conversion, 8-MHz readout, no corrections, and 14-bit depth, and 30-Hz rates were achieved at exposure times of 10–0.1 ms. The in-built SWIR light-emitting diode (LED, 940 nm) was used for SWIR white light (anatomical reference) images (10 ms). A red, green, blue LED with a 650-nm short-pass filter (FES0650; Thorlabs) provided ambient lighting (70 μW/cm^2 at 488 nm).

SWIR Spectral Measurement of pHLIP ICG

The NIR absorbance of pHLIP ICG was measured on a plate reader (SpectraMax iD5; Molecular Devices). pHLIP ICG's SWIR emission spectra were assessed with and without 1-palmitoyl-2-oleoyl-sn-glycero-3-phosphocholine liposomes (POPC) (100 nm; T&T Scientific Corp.; Fig. 1D) (*24*,*25*). SWIR spectra were acquired using a home-built SWIRFI spectroscopy system and tunable white light source (SuperK Extreme supercontinuum white light laser; NKT Photonics), an inverted microscope (IX-71 microscope and ×20 SWIR objective; Olympus), and a 1-dimensional indium gallium arsenide NIR detector (iDus 1.7-μm InGaAs, Andor; Oxford Instruments). Light was collected at exposures of 0.1–5 s with 808 nm excitation. Wavelength-dependent emission intensity artifacts from the spectrometer, detector, and other optics were corrected via an HL-3-CAL-EXT halogen calibration light source (Ocean Optics).

Phantom Imaging

Commercial imaging phantoms (ICG-equivalent Reference Set; Quel Imaging) assessed resolution, sensitivity, and depth penetration of NIRFI and SWIRFI preclinical systems (*34*–*36*). Quel targets were analyzed by Quel's dedicated site (*35*). Custom prelens filter mounts and appropriate long-pass filters (FELH-1100, FELH-1200, and FELH-1300 with SM1L03; Thorlabs) enabled SWIRFI at longer wavelengths of 1,100, 1,200, and 1,300 nm, respectively.

NIRFI

NIRFI was performed on a gold-standard commercial system (IVIS Spectrum CT; PerkinElmer). System settings were low binning, f-stop 1, high lamp, and 745- and 820-nm excitation and emission filter sets, respectively. Raw (luminescent) tiff files were analyzed after dark-noise subtraction, with median filtering (outlier removal) and gaussian blur applied as for SWIRFI. Exposure times ranged from 10 to 10,000 ms.

Image Processing and Analysis

SWIRFI data (h5 format) were converted to 14-bit tiff files in ImageJ (*37*). Automated image processing consisted of dark-noise subtraction and 32-bit conversion, flat field correction with a normalized ICG (Cardiogreen, I2633; Sigma) image, dark and bright pixel removal via median filtering (outlier removal; kernel, 1; threshold, 500), LUT (Fire) application, gaussian blur (σ = 2 pixels), and thresholding. Single frames were quantified for all exposures. Analysis was performed in GraphPad Prism (version 9.3.1; GraphPad Software) and MATLAB

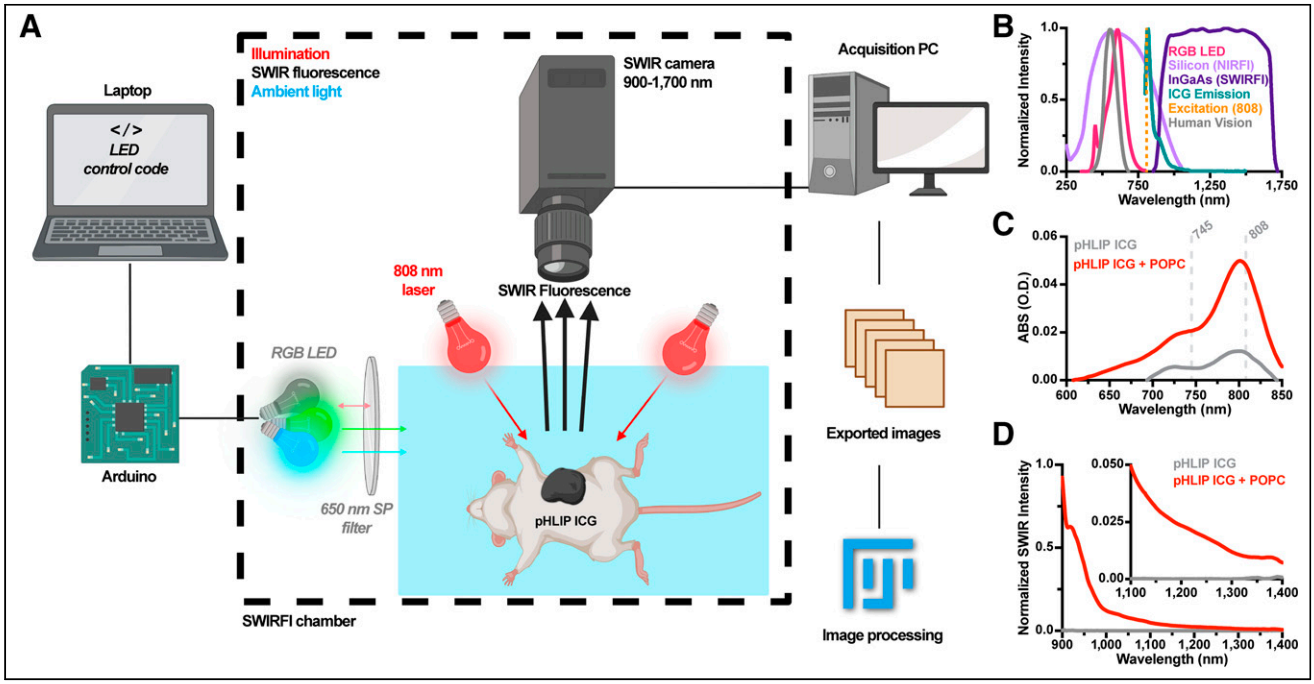

FIGURE 1. Ambient light resistant SWIRFI for pHLIP ICG detection. (A) SWIRFI setup for ambient light resistant imaging of pHLIP ICG. Images were automatically converted to tiff files for rapid image correction and analysis (ImageJ). Panel was created with Biorender.com. (B) Comparison of silicon (NIRFI), indium gallium arsenide (InGaAs; SWIRFI) sensors, and human vision responses with ICG laser excitation (808 nm), ICG, and LED emission profiles. (C) pHLIP ICG absorption (100 μL, 8 μM) with and without (bound and unbound) POPC liposomes. NIRFI (745 nm) and SWIRFI (808 nm) excitation wavelengths are shown. (D) SWIR emission of pHLIP ICG (normalized) in on and off states. (Inset) Emission from 1,100 to 1,400 nm. ABS (O.D.) = absorbance (optical density); PC = personal computer; RGB = red, green, blue; SP = short pass.

(2021b; MathWorks). SNR and CNR values (dB) were calculated (Excel, version 16.57; Microsoft) according to Equations 1 and 2:

$$\mathrm{SNR_{dB}} = 10 \times \log_{10}\left(\frac{\text{brightest ROI}_{\mathrm{Avg}} - \text{background ROI}_{\mathrm{Avg}}}{\text{background ROI}_{\mathrm{SD}}}\right) \quad \text{Eq. 1}$$

$$\mathrm{CNR_{dB}} = 10 \times \log_{10}\left(\frac{\text{tumor ROI}_{\mathrm{Avg}} - \text{body ROI}_{\mathrm{Avg}}}{\text{body ROI}_{\mathrm{SD}}}\right). \quad \text{Eq. 2}$$

Mouse Handling

Mouse handling, imaging, and housing were performed in accordance with the National Institutes of Health guidelines and approved by the Office of the Institutional Animal Care and Use Committee protocols at Memorial Sloan Kettering Cancer Center. Athymic female nude mice (n = 12, Foxn1^{nu}, 002019, inbred; the Jackson Laboratory) were housed under a 12-h on-and-off light cycle, with up to 5 mice per cage with food (trimethoprim–sulfamethoxazole [Sulfatrim] addition; TestDiet, #TD1810356-293) and water ad libitum. Mammary fat pad injection of 3.0 × 10^5 4T1 cells (ATCC, CRL-2539, STR-validated, *Mycoplasma*-free) suspended in 30 μL of Matrigel generated orthotopic breast tumor models. At tumor sizes of approximately 100 mm^3 (~7–9 d postinjection), mice intravenously received pHLIP ICG (0.5 mg/kg) and were imaged 1, 24, 48, 72, and 96 h after injection. Anesthesia was achieved in all cases via gaseous isoflurane inhalation (induction, 3%; maintenance, 1%–2% v/v). Euthanasia via CO_2 inhalation occurred at 96 h under approved protocols. Tumor resection (after euthanasia) was performed, with tumor excision confirmed via SWIRFI. SWIRFI necropsy biodistribution was performed for tumor, liver, kidneys, spleen, stomach, large and small intestines, brain, skin, bone, muscle, heart, and lungs. SWIRFI organ values from a noninjected (control) mouse were subtracted from injected mouse values. Two mice were excluded from all analyses because of a failed acquisition time point and insufficient tumor size, respectively. Hematoxylin and eosin (H&E) staining was performed in line with Supplemental Table 1 (supplemental materials are available at http://jnm.snmjournals.org).

RESULTS

Ambient Light Resistant SWIRFI for pHLIP ICG

SWIRFI's ambient lighting resistant setup and processing workflow were determined (Figs. 1A and 1B; Supplemental Fig. 1). Red, green, blue LED combinations without laser excitation found that green, blue, and green-blue (cyan) with and without a 650-nm short-pass filter and without gating were invisible to the sensor (there was no long-pass filter on the sensor; Supplemental Fig. 1). Red emission was barely detectable at 10 ms exposures (~5% of the sensor's dynamic range) and slightly dimmed by the 650 nm short-pass filter (Supplemental Fig. 1). The sensor's spectral response, human vision response, LED emission, laser excitation, and ICG emission combine to achieve ambient lighting resistant imaging under these conditions (Fig. 1B). pHLIP ICG NIR absorbance and SWIR emission spectra were determined on respective dedicated spectrometers (Figs. 1C and 1D). An 8 μM bound (with POPC liposomes) pHLIP ICG solution displayed characteristic ICG absorption (with a 802-nm peak). pHLIP ICG's SWIR fluorescence mechanism was in line with its previously reported NIR format and extended to approximately 1,400 nm, like that of naïve ICG, with the unbound solution, free of POPC liposomes, having minimal absorption or fluorescence, as expected (Figs. 1C and 1D) (*24*,*25*).

SWIRFI Advantages for pHLIP ICG

Phantoms enabled direct comparison between SWIRFI and NIRFI modalities in their ICG-optimized modes. Preclinical gold-standard NIRFI was performed on an IVIS system and found to be insensitive compared with SWIRFI. ICG-mimicking phantoms highlighted SWIRFI's improved sensitivity, improved depth (5.24 vs. 3.64 mm), and comparative resolution levels (2.5 line pairs/mm; Supplemental Fig. 2). This improvement was also found in custom pHLIP ICG phantoms in which SWIRFI had 100 times more sensitivity than NIRFI, both with and without tissue (Supplemental Fig. 3). SWIRFI achieved picomolar (0.4 nM) pHLIP ICG sensitivity at 10 ms (100 Hz equivalent) exposure times (Supplemental Fig. 4), at a third of the American National Standards Institute limit for laser fluence at 808 nm (ANSI, <330 mW/cm^2) (*38*).

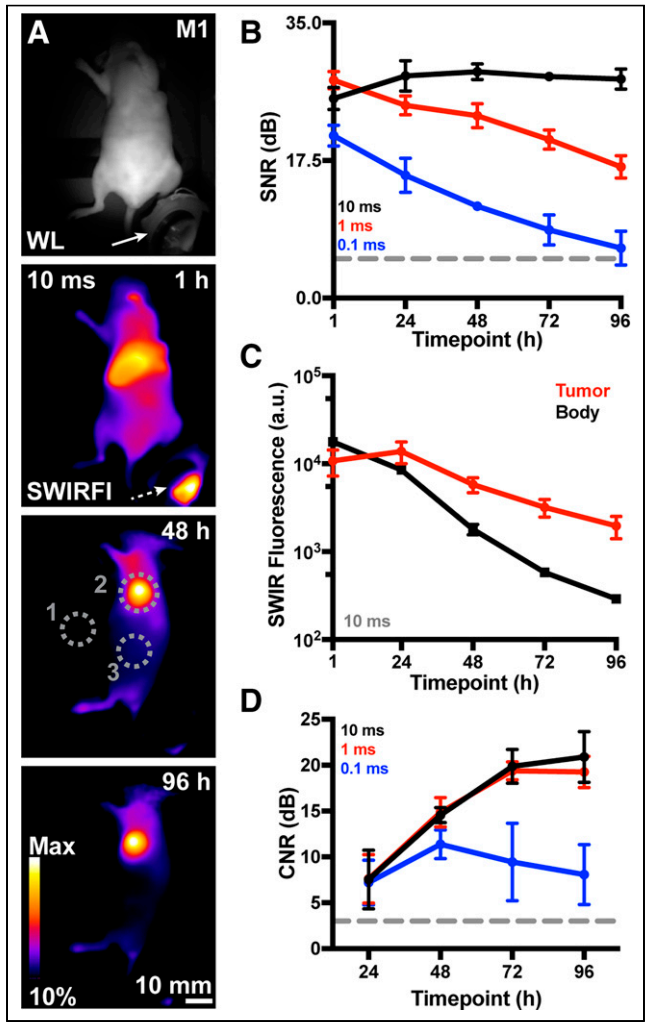

FIGURE 2. Ambient lighting resistant SWIRFI tumor screening via pHLIP ICG. (A) Representative white light (WL, in-built SWIR LED illumination, 940 nm) and SWIRFI detection of pHLIP ICG–injected mice (>900 nm, n = 4, 10 ms, 0.5 mg/kg) at 1, 48, and 96 h after injection. Negligible signal was detected from a control mouse (data not shown, noninjected, n = 1). (B) SNR (dB) of brightest point from all mice from 1 to 96 h at all exposures (10, 1, and 0.1 ms). (C) Values (10 ms) comparing tumor and body SWIRFI levels. Tumor fluorescence peaked at 24 h and was retained up to 96 h. (D) Tumor-to-body CNR (dB) increases past 24 h and peaks at 72 h. In all cases, mean and SD are shown (n = 4 biologic replicates) aside from D, up to 96 h with 0.1 ms exposure, where only n = 3 values are shown. a.u. = arbitrary unit; dotted arrow = fluorescence reflection from ambient LED; dotted gray circles = quantification regions of interest, where 1 is system noise (SNR), 2 is tumor values, and 3 is body values (CNR); Dotted line = acceptable thresholds (5 dB for SNR, 3 dB for CNR); M1 = mouse 1; Max = maximum; solid arrow = ambient light source (red, green, blue LED).

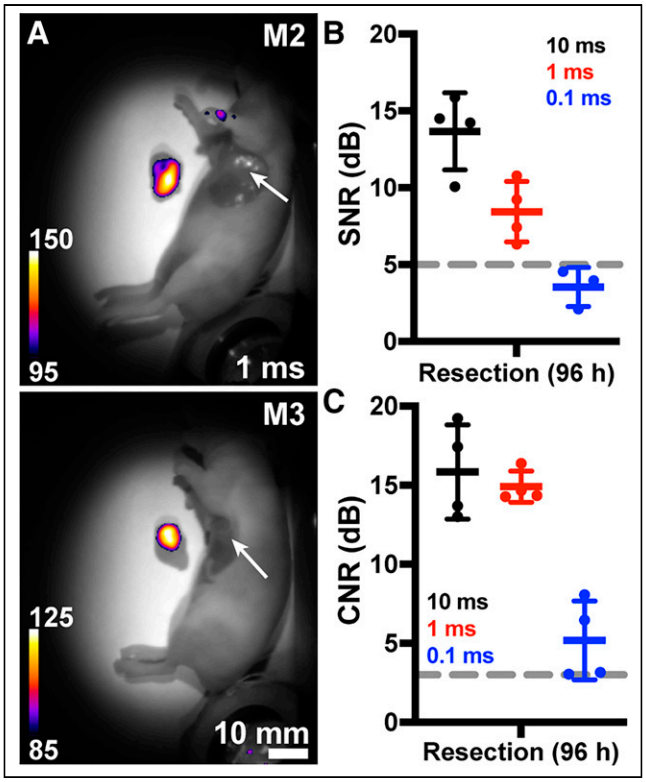

FIGURE 3. Ambient lighting resistant SWIRFI resection. (A) Representative SWIRFI white light (WL) overlaid with detection of tumor resection (after euthanasia) at 96 h. The tumor is clearly delineated from both the body and tumor bed (arrow). (B) Resected tumor SNR levels for all exposure times. (C) Resected tumor CNR levels for all exposure times. In all cases, mean and SD are shown (n = 4 biologic replicates, aside from B, 0.1 ms exposure, where only n = 3 are shown). Dotted line = acceptable thresholds (5 dB for SNR, 3 dB for CNR); M2 = mouse 2; M3 = mouse 3.

Improved Tumor Contrast via SWIRFI Under Ambient Lighting

Reanalysis of 0 to 48 h published NIRFI levels for pHLIP ICG biodistribution found competition between tumor and liver fluorescence, and after 48 h, tumor contrast should improve (Supplemental Fig. 5) (*24*). Because SWIRFI provided sufficient (picomolar) sensitivity to detect low probe levels, we assessed tumor contrast up to 96 h after injection. Nude mice bearing orthotopic breast tumors were used for facile SWIRFI of deep-seated organs through the skin (*24*). pHLIP ICG was administered intravenously (0.5 mg/kg), with SWIRFI performed every 24 h from 1 to 96 h. Signal collection from the deep-seated liver was aided by imaging above the ANSI fluence limit at 808 nm (450 mW/cm^2), removing the need to euthanize mice at later time points (*38*). SWIRFI of pHLIP ICG and the image processing pipeline displayed excellent tumor screening from 24 to 96 h (Fig. 2; Supplemental Figs. 6 and 7). As expected, liver fluorescence was strongest 1 h after injection, decreasing with time as tumor contrast and delineation simultaneously increased. SWIRFI consistently performed with high SNR values (~30 dB, 10 ms) above acceptable 5 dB thresholds (Fig. 2B). Tumor fluorescence levels peaked at 24 h compared with surrounding areas, with CNR values also above acceptable 3 dB thresholds. However, CNR values dramatically increased, peaking from 72 to 96 h with 10- and 1-ms exposures providing indistinguishable CNR values. A batch of mice imaged within the ANSI limit (300 mW/cm^2 at 808 nm) provided similar results (Supplemental Fig. 8) to aid clinical translation of these results. Gold-standard NIRFI required exposure of 1,000 ms to match the 1 ms SWIRFI SNR and CNR (Supplemental Fig. 9).

SWIRFI Tumor Resection via pHLIP ICG Under Ambient Lighting

Surgical resection (after euthanasia) was performed at 96 h. SWIRFI binarily delineated the tumor (Fig. 3A) and confirmed tumor-free beds with SNR and CNR above acceptable thresholds (Figs. 3B and 3C). SWIRFI biodistribution found tumors had significantly higher fluorescence than other tissues, confirming the improved clearance of pHLIP ICG from tissues other than the tumor (Fig. 4). Values for all organs from all mice are shown (Fig. 4), as are all organs with corresponding threshold levels from all mice (Supplemental Fig. 10). Images and values are combined from mice imaged at 808 nm fluence levels of either 450 or 300 mW/cm^2, with each corrected via noninjected organs. H&E staining was performed on select organs, confirming the characterization of tissues associated with residual agent uptake (Supplemental Fig. 11).

Extended SWIRFI (>1,100 nm) of pHLIP ICG In Vivo

We then investigated the emission of pHLIP ICG extended past 1,100 nm in vivo (Fig. 1D), similar to antibody-conjugated ICG imaging (*39*). First, a 4 μM pHLIP ICG solution with POPC liposomes, as before, was imaged in a multiwell plate. Imaging was performed with and without scattering medium (raw chicken breast) and various long-pass optical filters (Supplemental Fig. 12). A reduction of 1.98 mm in the full width at half maximum was found when imaging with a long-pass filter at 1,100 nm over 900 nm (no filter and sensor spectral response). This was further reduced by 2.27 mm when employing

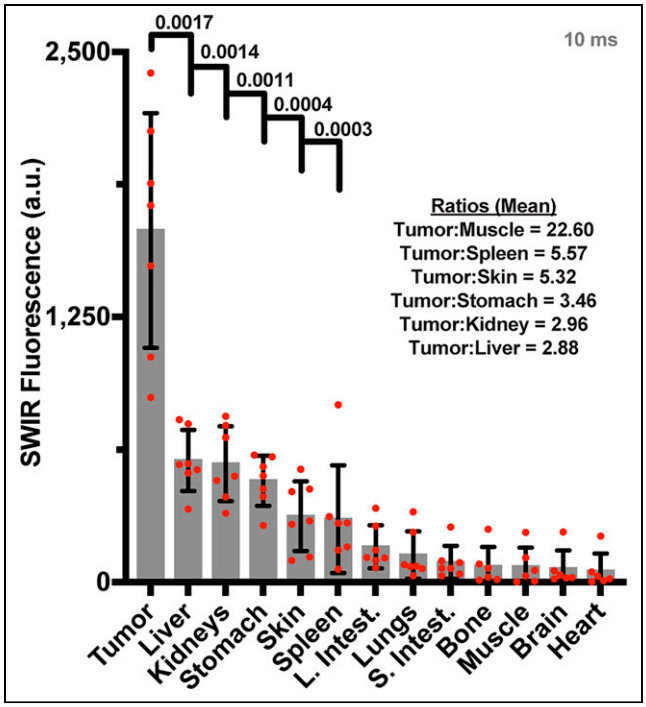

FIGURE 4. Ambient lighting resistant SWIRFI necropsy biodistribution. SWIRFI organ values. Respective endogenous values from control mice imaged under comparative conditions have been subtracted for each. Mean, standard deviation, and biologic replicates (n = 7) are shown, negative values after endogenous level subtraction are not shown. Select P values (<0.05, Welch 2-tailed t test, unpaired, parametric) and ratios comparing tumor to select tissues are shown. a.u. = arbitrary unit; L. Intest. = large intestine; S. Intest. = small intestine.

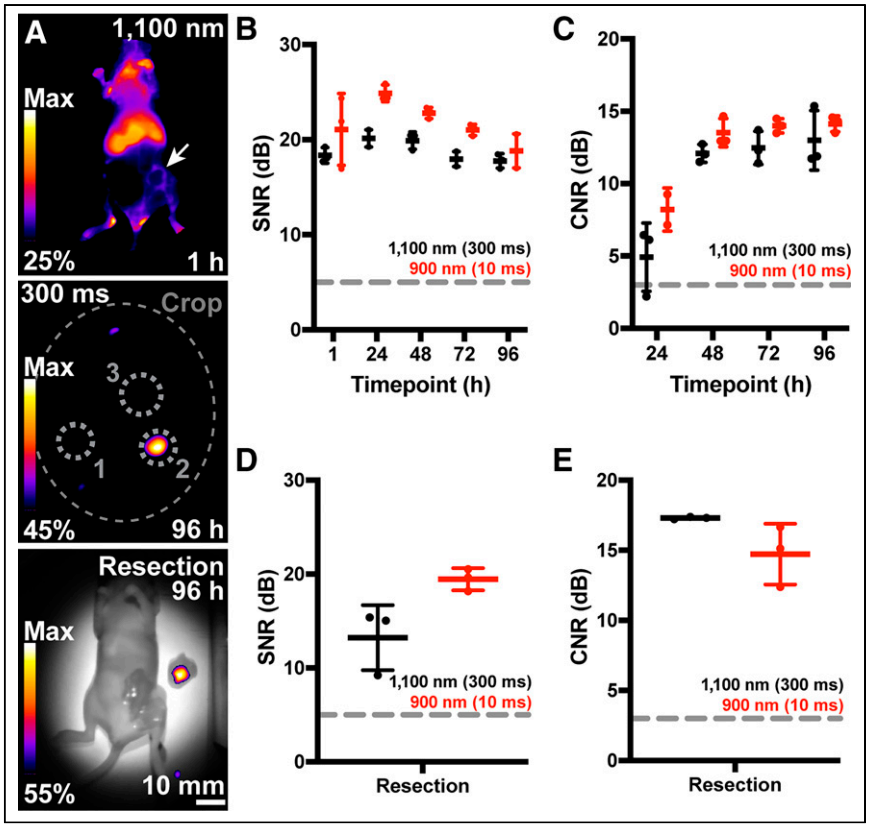

FIGURE 5. Ambient lighting resistant extended emission SWIRFI (>1,100 nm) of pHLIP ICG in vivo. (A, top) >1,100 nm representative image 1 h after pHLIP ICG (300 ms, 0.5 mg/kg). Gaussian blur has not been added to 1 h time point images. (A, middle) >1,100 nm image at 96 h. Regions of interest are shown as before. (A, bottom) >1,100 nm SWIRFI resection for complete tumor removal at 96 h. (B) SNR values of >1,100 nm (300-ms exposure) and >900 nm (10-ms exposure) from all mice at all time points. Exposures were selected at close to camera saturation at 1 h and then used for all time points. (C) Tumor CNR values from 24 to 96 h from all mice. (D and E) Comparative resection SNR and CNR values at both >1,100 and >900 nm for all mice. SD, mean, and individual replicates (n = 3) are shown. a.u. = arbitrary units; dotted gray circles = quantification regions of interest, where 1 is system noise (SNR), 2 is tumor values, and 3 is body values (CNR); large dotted gray oval = cropping because of long-pass filter; dotted lines = acceptable thresholds (5 dB for SNR, 3dB for CNR); Max = maximum; solid arrow = tumor location.

a long-pass filter at 1,300 nm. A final batch of mice was imaged using the 1,100 nm long-pass filter after pHLIP ICG administration, as before, with the extended SWIRFI emission of pHLIP ICG readily detected, albeit not at video rates (Fig. 5; Supplemental Figs. 13 and 14).

DISCUSSION

In this work, preclinical commercial SWIRFI's advantages for pHLIP ICG were shown in phantoms, along with its utility in tumor screening and resection. When compared in their respective ICG optimized modes, SWIRFI consistently outperformed a NIRFI system. The used SWIRFI system and developed image processing pipeline produced relevant and accurate images (Figs. 1–3 and 5; Supplemental Figs. 6–8, 10, and 13). The achieved sensitivity (Supplemental Figs. 2–4) facilitated video rate tumor detection, guided resection, and determined biodistribution at low probe levels up to 96 h after injection, highlighted by the high SNR and CNR levels at exposure times of 10, 1, and 0.1 ms (Figs. 2–4). The video rate picomolar sensitivity of SWIRFI was essential for validating the hypothesized increase in tumor CNR at later time points (Supplemental Fig. 4; Supplemental Video 1). The next iterations could use the minor decrease in SNR with comparative CNR at 1 versus 10 ms (Figs. 2 and 3), with gated laser emission to reduce exposure of the agent at no cost to tumor delineation, thus reducing photobleaching (*40–43*). The mean necropsy-based muscle-to-tumor ratio of 22.6 at 96 h provided binary and unambiguous tumor delineation, with tumor values that were statistically significant compared with liver values (Fig. 4; Supplemental Fig. 10). Considering the wide tumor-targeting capabilities of pHLIP ICG, other tumor models should be investigated (*24*).

All SWIRFI images and results presented here were performed under ambient lighting conditions with no detriment to signal accuracy (*17,18*). The LED (~$1) used in a green-blue combination was undetectable by the sensor with and without filtering (Fig. 1; Supplemental Fig. 1). This proof-of-principle work positions SWIRFI as an easily scalable, cost-effective, environmentally friendly, and democratic facile solution for ambient light resistant fluorescence guided surgery (FGS) without gating or filters (*33*). Future iterations should aim to assess various commercial LEDs for clinical deployment.

The spectral emission of pHLIP ICG extended past 1,100 nm is also shown. A direct comparison was made from mice consecutively imaged with 900 (sensor response) and 1,100 nm long-pass filters at all time points (Fig. 5; Supplemental Figs. 13 and 14). However, the 1,100-nm cutoff did not equate to an improved SNR or CNR over the 900 nm cutoff images because of tumor localization of pHLIP ICG at later time points, topical tumor location, and overall reduction in bulk sensitivity above 1,100 nm. SWIRFIs resolution improvement (>1,100 or >1,300 nm) is likely of more benefit to smaller-structure imaging (angiography, delineation of nerves, micrometastases) than to large tumor masses (*8,15*).

These results have implications for preclinical imaging, in which novel targeting agents (peptides, nanoparticles, small molecules, antibodies, etc.) can be evaluated via video rate SWIRFI by conjugating ICG, or novel SWIRFI dyes can be evaluated using the pHLIP (*16,44*). The achieved sensitivity may permit dose reduction for detection and simultaneously elongate imaging windows—improving tumor delineation (CNR), as shown here—and could be combined with multispectral SWIRFI for even further improvement (*45*). Clinical translation of the observed CNR increase could enable democratic dissemination of tumor resection techniques, with nonexperts (as in this work) being able to perform targeted FGS, with resection ambiguity being simultaneously eliminated for experienced surgeons. The ability to perform guided resection under ambient lighting via SWIRFI with minimal disruption to current workflows may aid surgeon uptake of FGS. The potential for direct clinical translation of these results has been established via laser intensities within the ANSI limit

(<330 mW/cm^2; Supplemental Fig. 8). However, this translation will require a custom SWIRFI device with a smaller footprint than current preclinical systems, as well as improvements in usability. Such a device should also be compared with current clinical NIRFI systems. At the time of writing, no SWIRFI device has received Food and Drug Administration approval or is routinely deployed clinically, especially in complex operating room environments. In addition, the LED setup should be scaled up for ambient lighting.

CONCLUSION

This work validates a pH-sensitive, peptide-based, tumor-targeting agent conjugated to ICG, which is in clinical trials, for SWIRFI. pHLIP conjugation to ICG retains both pHLIP's tumor selective mechanism and the extended emission of ICG in the SWIR region, where tissue scattering, absorbance, and autofluorescence are minimal (Figs. 1, 2, and 5; Supplemental Fig. 12) (*24*). Accordingly, SWIRFI was readily performed with minimal to no background interference from tissue and under ambient lighting conditions. SWIRFI provided unprecedented CNR and SNR at various exposure times (10–0.1 ms) that are at least 3 and up to 300 times faster than video rate requirements (30 ms). Combining SWIRFI sensitivity with extended probe clearance provides unambiguous and binary tumor delineation resistant to ambient lighting. This work calls for a clinically compatible system to further assess SWIRFI for clinical FGS. Such a system could provide video rate FGS under ambient lighting conditions at improved tissue depth and resolution with high confidence in complete tumor resection. This may have clinical implications for tumor visualization through blood pools or in highly optically scattering tissue environments, for example, brain gliomas or lymphatic mapping (*5*,*22*,*46*).

DISCLOSURE

This work was supported by the NIH (R56 EB030512 to Jan Grimm, R35 CA232130 to Jason Lewis, and F32 CA268912-01 to Edwin Pratt), the National Science Foundation CAREER Award (1752506 to Daniel Heller), the NCI (R01-CA215719 to Daniel Heller and Cancer Center Support Grant P30-CA008748, Selwyn Vickers/MSKCC), the NIBIB (R01-EB033651 to Daniel Heller), the American Cancer Society Research Scholar Grant (GC230452 to Daniel Heller), the Louis and Rachel Rudin Foundation (to Daniel Heller), the Experimental Therapeutics Center of MSKCC (to Daniel Heller), Mr. William H. Goodwin and Mrs. Alice Goodwin and the Commonwealth Foundation for Cancer Research (to Daniel Heller). Mijin Kim was supported by the NIH (K99-EB033580) and the Marie-Josée Kravis Women in Science Endeavor Postdoctoral Fellowship. Jason Lewis is a founder of and has shares in pHLIP, Inc. pHLIP, Inc. has provided funding for manufacturing of pHLIP ICG, safety, pharmacology, and toxicology studies and donated pHLIP ICG for this study. Jason Lewis has shares in Stryker Corp. Daniel Heller is a cofounder and officer with equity interest in Lime Therapeutics, Inc., and cofounder with equity interest in Selectin Therapeutics Inc. and Resident Diagnostics, Inc., and a member of the scientific advisory board of Concarlo Therapeutics, Inc., Nanorobotics Inc., and Mediphage Bioceuticals, Inc. No other potential conflict of interest relevant to this article was reported.

ACKNOWLEDGMENTS

We thank pHLIP, Inc., for the donation of pHLIP ICG to this investigation. The authors also thank the support of Memorial Sloan Kettering Cancer Center's Animal Imaging Core Facility.

KEY POINTS

QUESTION: Does pHLIP ICG, a cancer-targeting agent currently in clinical trials for FGS, serve as a suitable candidate for SWIRFI?

PERTINENT FINDINGS: This work compared commercially available preclinical systems in their optimized ICG detection modes and found SWIRFI readily outperformed the current NIRFI gold standard for both depth and sensitivity.

IMPLICATIONS FOR PATIENT CARE: The picomolar sensitivity of SWIRFI enabled video rate imaging of pHLIP ICG at lengthy time points (96 h). This resulted in a dramatic improvement in CNR, providing binary and unambiguous tumor delineation that was unaffected by ambient light. This work is a direct precedent for clinical SWIRFI deployment for tumor resection and has implications for preclinical probe development.

REFERENCES

1. Thimsen E, Sadtler B, Berezin MY. Shortwave-infrared (SWIR) emitters for biological imaging: a review of challenges and opportunities. *Nanophotonics.* 2017;6:1043–1054.
2. Vollmer M, Möllmann K-P, Shaw JA. The optics and physics of near infrared imaging. Paper presented at: Education and Training in Optics and Photonics; 2015; Bordeaux, France.
3. McLarney BE, Zhang Q, Pratt EC, et al. Detection of shortwave-infrared Cerenkov luminescence from medical isotopes. *J Nucl Med.* 2022;64:177–182.
4. Qi J, Sun C, Zebibula A, et al. Real-time and high-resolution bioimaging with bright aggregation-induced emission dots in short-wave infrared region. *Adv Mater.* 2018;30:e1706856.
5. Byrd BK, Marois M, Tichauer KM, et al. First experience imaging short-wave infrared fluorescence in a large animal: indocyanine green angiography of a pig brain. *J Biomed Opt.* 2019;24:080501.
6. Jacques SL. Optical properties of biological tissues: a review. *Phys Med Biol.* 2013;58:R37–R61.
7. Golovynskyi S, Golovynska I, Stepanova LI, et al. Optical windows for head tissues in near-infrared and short-wave infrared regions: approaching transcranial light applications. *J Biophotonics.* 2018;11:e201800141.
8. Carr JA, Aellen M, Franke D, So PT, Bruns OT, Bawendi MG. Absorption by water increases fluorescence image contrast of biological tissue in the shortwave infrared. *Proc Natl Acad Sci USA.* 2018;115:9080–9085.
9. Wang F, Ren F, Ma Z, et al. In vivo non-invasive confocal fluorescence imaging beyond 1,700 nm using superconducting nanowire single-photon detectors. *Nat Nanotechnol.* 2022;17:653–660.
10. Hong G, Antaris AL, Dai H. Near-infrared fluorophores for biomedical imaging. *Nat Biomed Eng.* 2017;1:0010.
11. Wang F, Qu L, Ren F, et al. High-precision tumor resection down to few-cell level guided by NIR-IIb molecular fluorescence imaging. *Proc Natl Acad Sci USA.* 2022;119:e2123111119.
12. Carr JA, Franke D, Caram JR, et al. Shortwave infrared fluorescence imaging with the clinically approved near-infrared dye indocyanine green. *Proc Natl Acad Sci USA.* 2018;115:4465–4470.
13. Cosco ED, Lim I, Sletten EM. Photophysical properties of indocyanine green in the shortwave infrared region. *ChemPhotoChem.* 2021;5:727–734.
14. Carr JA, Valdez TA, Bruns OT, Bawendi MG. Using the shortwave infrared to image middle ear pathologies. *Proc Natl Acad Sci USA.* 2016;113:9989–9994.
15. Wu Y, Suo Y, Wang Z, et al. First clinical applications for the NIR-II imaging with ICG in microsurgery. *Front Bioeng Biotechnol.* 2022;10:1042546.
16. Bandi VG, Luciano MP, Saccomano M, et al. Targeted multicolor in vivo imaging over 1,000 nm enabled by nonamethine cyanines. *Nat Methods.* 2022;19:353–358.
17. Cosco ED, Arús BA, Spearman AL, et al. Bright chromenylium polymethine dyes enable fast, four-color in vivo imaging with shortwave infrared detection. *J Am Chem Soc.* 2021;143:6836–6846.
18. Zhang L, Shi X, Li Y, et al. Visualizing tumors in real time: a highly sensitive PSMA probe for NIR-II imaging and intraoperative tumor resection. *J Med Chem.* 2021;64:7735–7745.

19. Hu Z, Fang C, Li B, et al. First-in-human liver-tumour surgery guided by multispectral fluorescence imaging in the visible and near-infrared-I/II windows. *Nat Biomed Eng.* 2020;4:259–271.
20. Shi X, Zhang Z, Zhang Z, et al. Near-infrared window II fluorescence image-guided surgery of high-grade gliomas prolongs the progression-free survival of patients. *IEEE Trans Biomed Eng.* 2022;69:1889–1900.
21. Cao C, Deng S, Wang B, et al. Intraoperative near-infrared II window fluorescence imaging-assisted nephron-sparing surgery for complete resection of cystic renal masses. *Clin Transl Med.* 2021;11:e604.
22. Teng CW, Cho SS, Singh Y, et al. Second window ICG predicts gross-total resection and progression-free survival during brain metastasis surgery. *J Neurosurg.* 2021;135:1026–1035.
23. Almuhaideb A, Papathanasiou N, Bomanji J. ^{18}F-FDG PET/CT imaging in oncology. *Ann Saudi Med.* 2011;31:3–13.
24. Crawford T, Moshnikova A, Roles S, et al. pHLIP ICG for delineation of tumors and blood flow during fluorescence-guided surgery. *Sci Rep.* 2020;10:18356.
25. Golijanin J, Amin A, Moshnikova A, et al. Targeted imaging of urothelium carcinoma in human bladders by an ICG pHLIP peptide ex vivo. *Proc Natl Acad Sci USA.* 2016;113:11829–11834.
26. Wyatt LC, Lewis JS, Andreev OA, Reshetnyak YK, Engelman DM. Applications of pHLIP technology for cancer imaging and therapy. *Trends Biotechnol.* 2017;35:653–664.
27. Pinker-Domenig, K. A study of multiparametric MRI and pHLIP® ICG in breast cancer imaging during surgery. ClinicalTrials.gov website. https://clinicaltrials.gov/study/NCT05130801. Updated June 15, 2023. Accessed July 25, 2023.
28. Roberts S, Strome A, Choi C, et al. Acid specific dark quencher QC1 pHLIP for multi-spectral optoacoustic diagnoses of breast cancer. *Sci Rep.* 2019;9:8550.
29. Bauer D, Visca H, Weerakkody A, et al. PET imaging of acidic tumor environment with ^{89}Zr-labeled pHLIP probes. *Front Oncol.* 2022;12:882541.
30. Hwang S-K, Tyszkiewicz C, Morin J, Point GR, Liu C-N. Novel in vivo and ex vivo hybrid in vivo imaging system (IVIS) imaging offers a convenient and precise way to measure the glomerular filtration rate in conscious mice. *J Pharmacol Toxicol Methods.* 2021;110:107084.
31. Spinelli AE, Kuo C, Rice BW, et al. Multispectral Cerenkov luminescence tomography for small animal optical imaging. *Opt Express.* 2011;19:12605–12618.
32. Ezra-Elia R, Obolensky A, Ejzenberg A, et al. Can an in vivo imaging system be used to determine localization and biodistribution of AAV5-mediated gene expression following subretinal and intravitreal delivery in mice? *Exp Eye Res.* 2018;176:227–234.
33. Sexton KJ, Zhao Y, Davis SC, Jiang S, Pogue BW. Optimization of fluorescent imaging in the operating room through pulsed acquisition and gating to ambient background cycling. *Biomed Opt Express.* 2017;8:2635–2648.
34. Davis SC, Pogue BW, Dehghani H, Paulsen KD. Contrast-detail analysis characterizing diffuse optical fluorescence tomography image reconstruction. *J Biomed Opt.* 2005;10:050501.
35. LaRochelle EPM, Streeter SS, Littler EA, Ruiz AJ. 3D-printed tumor phantoms for assessment of in vivo fluorescence imaging analysis methods. *Mol Imaging Biol.* 2023;25:212–220.
36. Ruiz AJ, Garg S, Streeter SS, et al. 3D printing fluorescent material with tunable optical properties. *Sci Rep.* 2021;11:17135.
37. Schindelin J, Arganda-Carreras I, Frise E, et al. Fiji: an open-source platform for biological-image analysis. *Nat Methods.* 2012;9:676–682.
38. American National Standards Institute. *American National Standard for Safe Use of Lasers.* Laser Institute of America; 2007.
39. Tsuboi S, Jin T. Shortwave-infrared (SWIR) fluorescence molecular imaging using indocyanine green–antibody conjugates for the optical diagnostics of cancerous tumours. *RSC Advances.* 2020;10:28171–28179.
40. Clutter ED, Chen LL, Wang RR. Role of photobleaching process of indocyanine green for killing neuroblastoma cells. *Biochem Biophys Res Commun.* 2022;589:254–259.
41. Yaqoob Z, McDowell EJ, Wu J, Heng X, Fingler JP, Yang C. Molecular contrast optical coherence tomography: a pump-probe scheme using indocyanine green as a contrast agent. *J Biomed Opt.* 2006;11:054017.
42. Holzer W, Mauerer M, Penzkofer A, et al. Photostability and thermal stability of indocyanine green. *J Photochem Photobiol B.* 1998;47:155–164.
43. Yeroslavsky G, Umezawa M, Okubo K, et al. Photostabilization of indocyanine green dye by energy transfer in phospholipid-PEG micelles. *J Photopolym Sci Technol.* 2019;32:115–121.
44. Lim I, Lin EY, Garcia J, et al. Shortwave infrared fluorofluorophores for multicolor in vivo imaging. *Angew Chem Int Ed Engl.* 2023;62:e202215200.
45. Waterhouse DJ, Privitera L, Anderson J, Stoyanov D, Giuliani S. Enhancing intraoperative tumor delineation with multispectral short-wave infrared fluorescence imaging and machine learning. *J Biomed Opt.* 2023;28:094804.
46. Takeuchi M, Sugie T, Abdelazeem K, et al. Lymphatic mapping with fluorescence navigation using indocyanine green and axillary surgery in patients with primary breast cancer. *Breast J.* 2012;18:535–541.